AGU PUBLICATIONS

*Geophysical Research Letters*

Supporting Information for

# An Eastward Current Encircling Mercury

Z. Shi[1,2]†, Z. J. Rong[1,2,3]*†, S. Fatemi[4], J. A. Slavin[5], L. Klinger[6], C. Dong[7,8], L. Wang[7,8], J. Zhong[1,2,3], J. M. Raines[5], M. Holmström[9], C. J. Yuan[1,2,3], S. Barabash[9] and Y. Wei[1,2,3]

[1]Key Laboratory of Earth and Planetary Physics, Institute of Geology and Geophysics, Chinese Academy of Sciences; Beijing 100029, China.

[2]College of Earth and Planetary Sciences, University of Chinese Academy of Sciences; Beijing, China.

[3]Mohe Observatory of Geophysics, Institute of Geology and Geophysics, Chinese Academy of Sciences; Beijing, China.

[4]Department of Physics at Umeå University; Umeå, Sweden.

[5]Department of Climate and Space Sciences and Engineering, University of Michigan; Ann Arbor, MI, USA.

[6]Beijing International Center for Mathematical Research, Peking University; Beijing, China.

[7]Princeton Plasma Physics Laboratory, Princeton University; Princeton, NJ, USA.

[8]Department of Astrophysical Sciences, Princeton University; Princeton, NJ, USA.

[9]Swedish Institute of Space Physics; Kiruna, Sweden.

*Corresponding author: Z. J. Rong (rongzhaojin@mail.iggcas.ac.cn)

†These authors contributed equally to this work.

## Contents of this file

Text S1 to S2
Figures S1 to S8
Tables S1

## Introduction

This file contains 2 texts, 8 figures and 1 table. Text S1 and Text S2 describe how current density is calculated from the view of particle motion and the magnetohydrodynamic equilibrium respectively. Figure S1 displays density, temperature and pressure distributions in the magnetic equatorial plane. Figure S2 shows data coverage of spacecraft. Figure S3 and Figure S7 provide more information from simulations. Figure S4 gives magnetic field records of two flybys and exhibits crosses of the boundary layer. Figure S5 and Figure S6 are current density distributions calculated in the two ways described by Text S1 and Text S2 respectively. Figure S8 is the averaged heliocentric distance distribution. Table S1 is the parameter details of the hybrid simulations shown in Figure S2.

**Text S1.**

Calculation of current density from particle motion. The current density can also be calculated from the motions of charged particles. The total current density arising from the drift of charged particles in a static dipole field should consist of the current of the magnetic gradient drift ($\boldsymbol{J}_{\nabla}$), the current of the magnetic curvature drift ($\boldsymbol{J}_{R}$), and the magnetization current ($\boldsymbol{J}_{M}$) due to the gradient of the total magnetic moment and the inhomogeneous magnetic field—that is, $\boldsymbol{J}=\boldsymbol{J}_{\nabla}+\boldsymbol{J}_{R}+\boldsymbol{J}_{M}$ (Parks, 2004). The three types of current are calculated as $\boldsymbol{J}_{\nabla}=\frac{N(\mu_i+\mu_e)}{B^2}(\boldsymbol{B}\times\nabla B)$, $\boldsymbol{J}_{R}=-\frac{2N(W_{i\parallel}+W_{e\parallel})}{B^4}[(\boldsymbol{B}\cdot\nabla)\boldsymbol{B}]\times\boldsymbol{B}$, and $\boldsymbol{J}_{M}=\nabla\times\boldsymbol{M}=-\nabla\times\left[\frac{N(\mu_i+\mu_e)}{B}\boldsymbol{B}\right]$, respectively, where $\mu=\frac{mv_\perp^2}{2B}=\frac{W_\perp}{B}$, $W_\perp=\frac{1}{2}mv_\perp^2=k_BT$, $W_\parallel=\frac{1}{2}mv_\parallel^2=\frac{1}{2}k_BT$, ($k_B$ is Boltzmann's constant), and $v_\perp$ and $v_\parallel$ are the components of thermal velocity perpendicular and parallel to the magnetic field, respectively. The subscripts $i$ and e represent ions and electrons respectively. Each type of current can be evaluated by the FIPS NTP dataset if both ions (assumed to be protons in the calculation) and electrons have the same density ($N$) and temperature ($T$). The contribution of each current component to the statistically derived eastward current by $\nabla\times\boldsymbol{B}$ at the magnetic equatorial plane is shown in Figure S5. If the plasma pressure is isotropic, it can be proved that the sum of $J_{\nabla}+J_{R}+J_{M}$ equals the diamagnetic current $\boldsymbol{J}=\frac{\boldsymbol{B}}{B^2}\times\nabla P$ (Parks, 2004).

**Text S2**

Calculation of current density from Magnetohydrodynamic (MHD) theory. Following classic MHD theory, the current density in magnetohydrodynamic equilibrium can be derived generally as $\boldsymbol{J}_{\perp} = \frac{\boldsymbol{B}}{B^2} \times \left[\nabla P_{\perp} + (P_{\parallel} - P_{\perp}) \frac{(\boldsymbol{B} \cdot \nabla)\boldsymbol{B}}{B^2}\right]$, which is equivalent to the sum of $J_{\nabla}+J_R+J_M$ in terms of particle motions (Parks, 2004). If the plasma pressure is isotropic, the current density becomes $\boldsymbol{J} = \frac{\boldsymbol{B}}{B^2} \times \nabla P$. In our calculation, the plasma pressure, $P$, was derived from the FIPS NTP dataset (Figure S6).

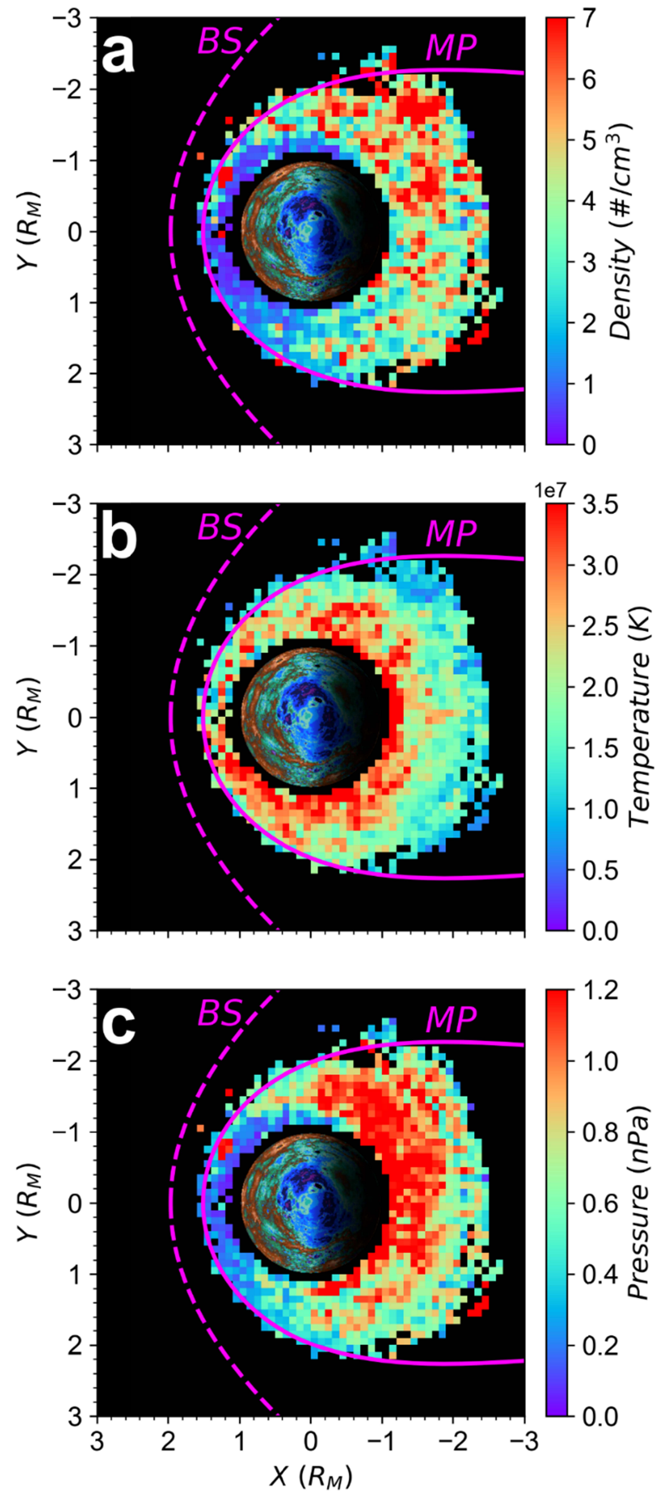


**Figure S1.** The distributions of proton number density, temperature and pressure in the magnetic equatorial plane ($|z|<0.05$ RM). **a, b** and **c** are the average distributions of number density, temperature and pressure derived from the FIPS NTP dataset (subsection 2.2), respectively.

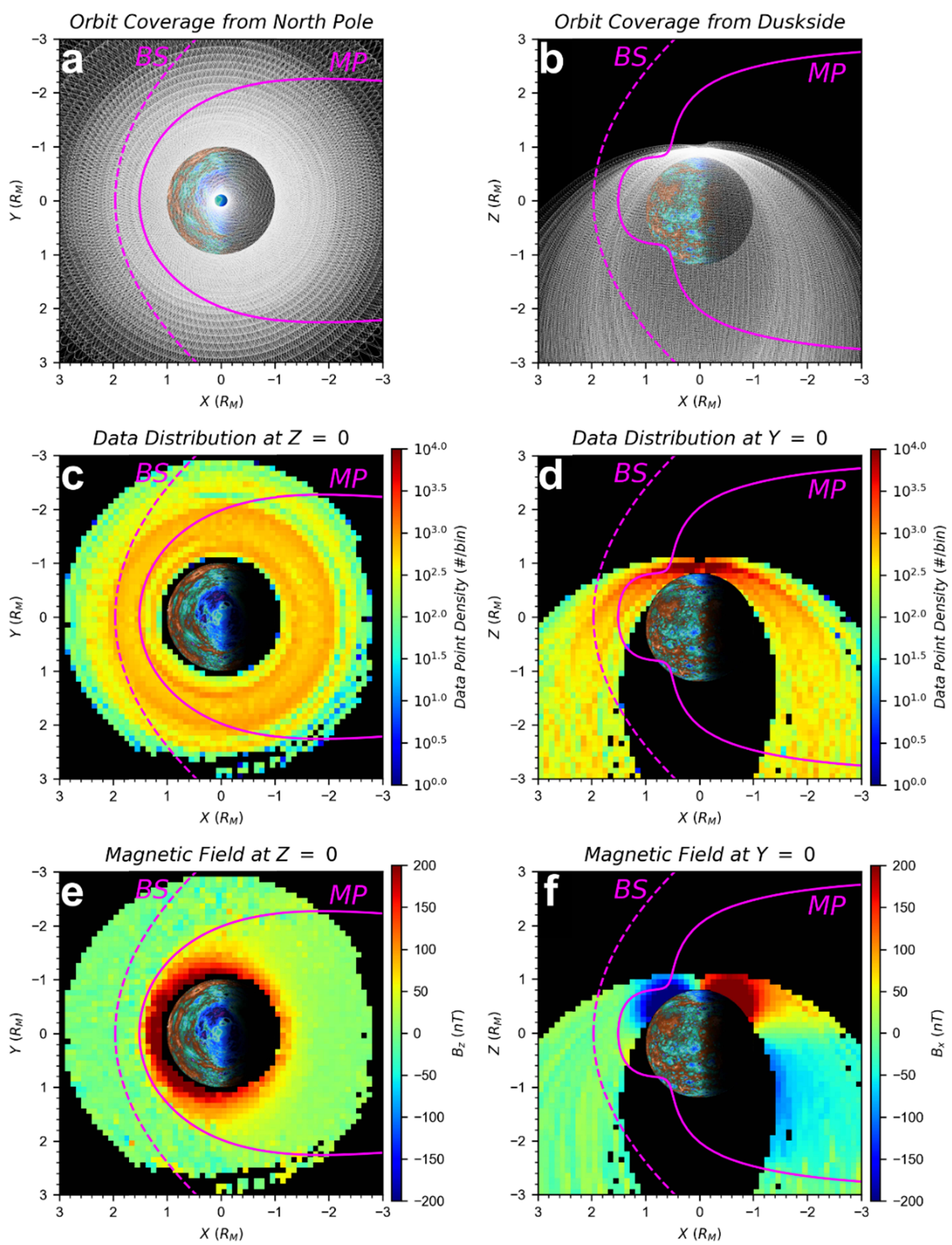


**Figure S2.** The overview of the distribution of spacecraft's trajectories, the density of sampled data points, and the sampled magnetic field. **a, b.** The projected trajectories of MESSENGER over the whole orbiting period (23 March 2011–30 April 2015) in the XY plane and XZ plane, respectively. **c, d.** The number density of data points in the cut of the magnetic equatorial plane ($|z|<0.05$ $R_M$) and meridian plane ($|y|<0.05$ $R_M$), respectively. **e.** The distribution of the magnetic field $B_z$ component in the cut of the magnetic equatorial plane. **f.** The distribution of the magnetic field $B_x$ component in the cut of the meridian plane. The magenta dashed and solid lines in each panel denote the nominal shape of the bow shock (Winslow et al., 2013) and magnetopause (Zhong et al., 2015), respectively.

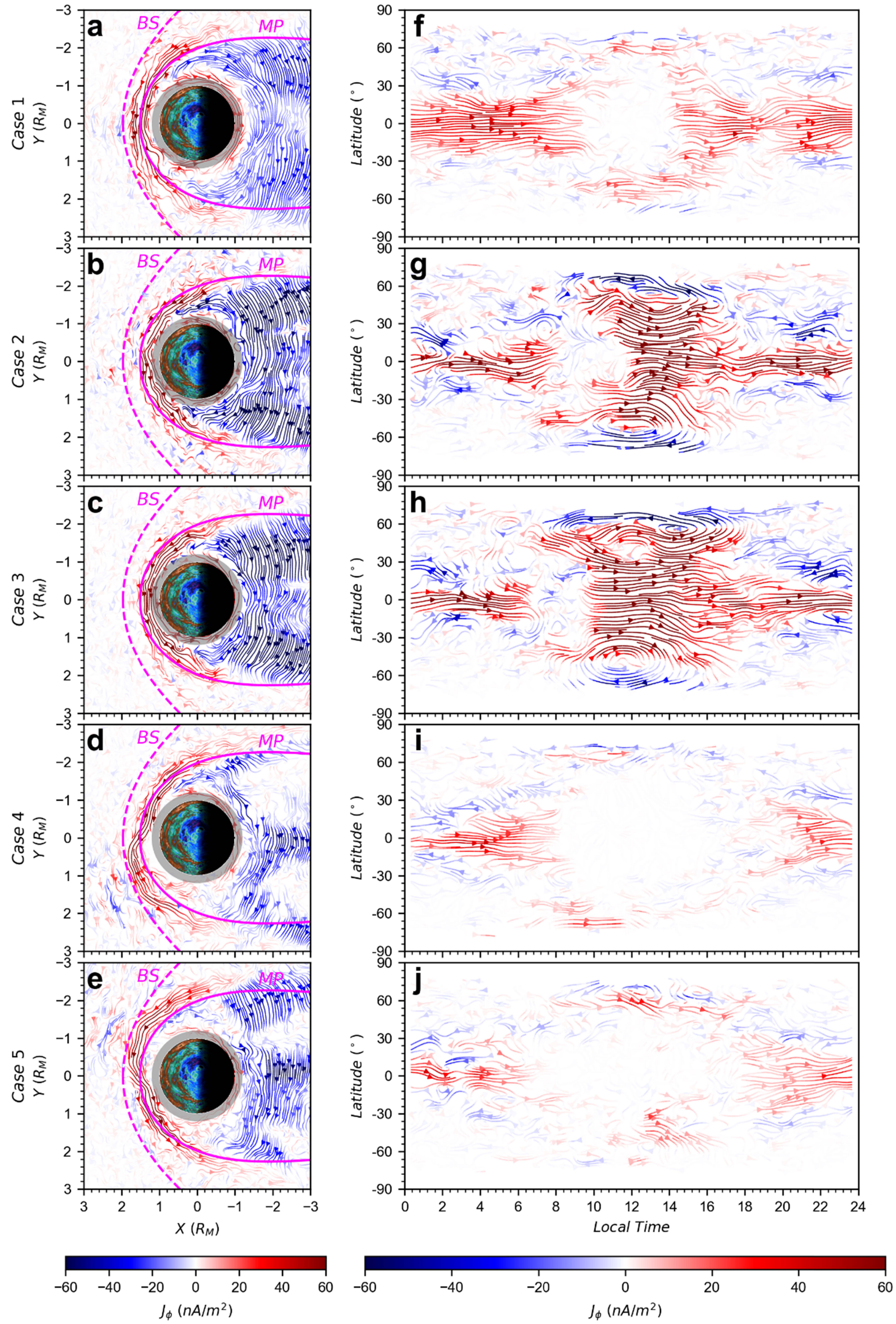


**Figure S3.** The simulated distributions of current density corresponding to the five cases tabulated in Table S1. **a–e.** The distributions of current density in the magnetic equatorial plane. **f–j.** The distributions of current density in the surface of a spherical shell covering radial distances of 1.0–1.2 $R_M$. The format for each case is the same as Figure 2.

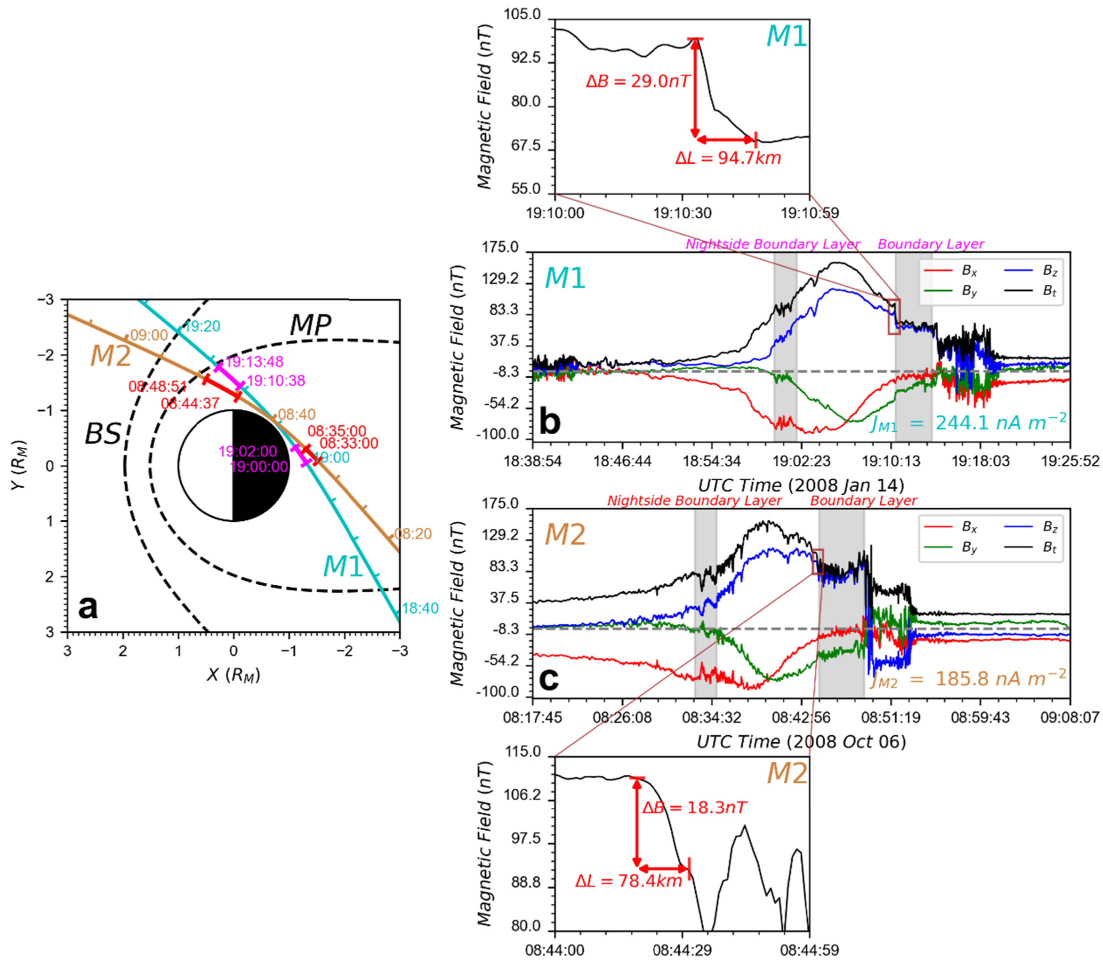


**Figure S4.** The recorded magnetic field by MESSENGER during the first two flybys. **a.** The trajectories of the first and second flybys projected in the equatorial plane. The lines colored by cyan and brown represent the trajectories of flyby 1 (M1) and flyby 2 (M2) respectively. The intervals of observed diamagnetic decreases are bolded with magenta for M1 and with red for M2. The trajectories for both flybys are nearly in the magnetic equatorial plane. **b.** The time series of the magnetic field during the period of M1. The intervals of significant diamagnetic decreases are shaded. The cut figure zooms in the interval when spacecraft experienced a steep fall of the field strength of 29.0 nT over a radial distance of $\Delta L$~94.7 km crossing the boundary layer of diamagnetic decrease during 19:10:38 – 19:13:48. The diamagnetic current at the boundary layer can be roughly estimated as $\boldsymbol{J \sim \mu_0^{-1}}\ \Delta B/\Delta L\ =\ \mathbf{244.1}\ \boldsymbol{nA\ m^{-2}}$. **c.** The time series of the magnetic field for M2. The format is the same with b. The estimated diamagnetic current for M2 during 08:44:37 – 08:48:51 is about $\mathbf{185.8}\ \boldsymbol{nA\ m^{-2}}$.

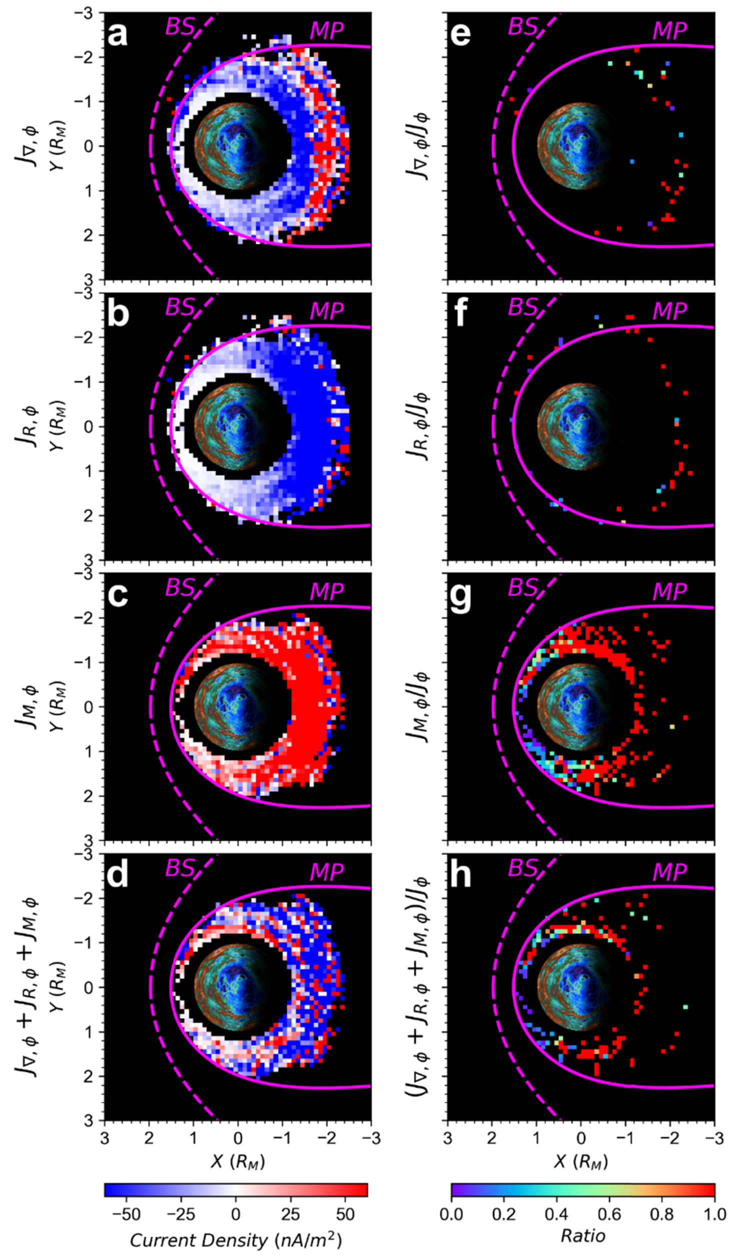


**Figure S5.** The calculated current density for different drift motions based on the FIPS NTP dataset, and the corresponding contributions to the statistically derived eastward current by $\boldsymbol{\nabla} \times \boldsymbol{B}$ in text. Both proton and electron are assumed with the same temperature and number density in calculation. **a–d.** The azimuthal components of current density carried by magnetic gradient drift, $\boldsymbol{J_{\nabla,\phi}}$ (**a**), magnetic curvature drift, $\boldsymbol{J_{R,\phi}}$ (**b**)**,** the magnetization current, $\boldsymbol{J_{M,\phi}}$ (**c**), as well as the sum of $\boldsymbol{J_{\nabla,\phi}} + \boldsymbol{J_{R,\phi}} + \boldsymbol{J_{M,\phi}}$ (**d**). The definition of each current can be found in Methods. **e–h.** The ratio of each current density correspondingly shown in **a–d** to the $\boldsymbol{J_\phi}$ derived by $\boldsymbol{\nabla} \times \boldsymbol{B}$ (Fig. 1) when the both current densities are eastward in a bin. Note, due to the sparse data coverage (Figure S1) and the possible break of guiding-center approximation in the faraway bins (distance beyond ~ 2 $R_M$), the calculated magnetic drift current might be meaningless therein.

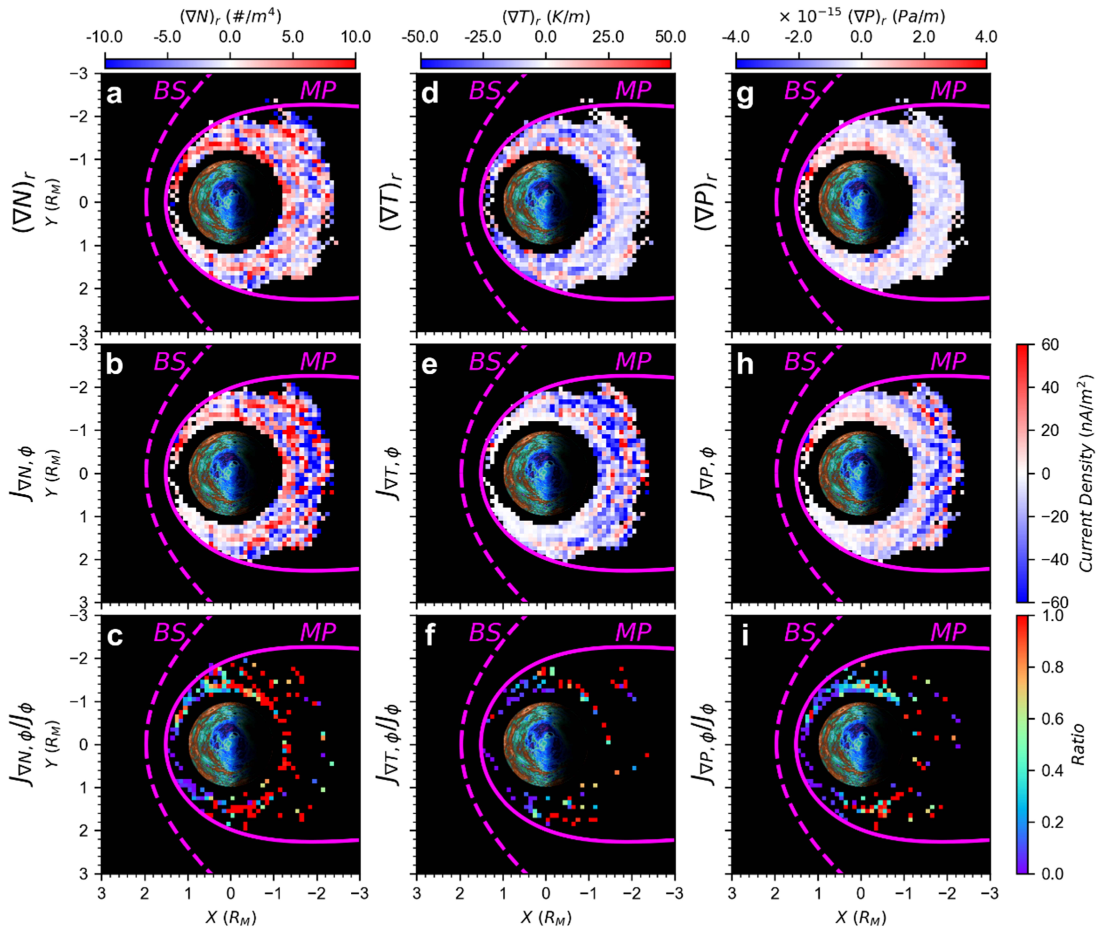


**Figure S6.** The contributions of the density gradient, temperature gradient, and the plasma pressure gradient to eastward current. Considering the diamagnetic current $\boldsymbol{J}_{\perp} = \frac{\boldsymbol{B}}{\boldsymbol{B}^2} \times \nabla \boldsymbol{P} = \frac{\boldsymbol{B}}{\boldsymbol{B}^2} \times \boldsymbol{k_B}(\boldsymbol{T}\nabla \boldsymbol{n} + \boldsymbol{n}\nabla \boldsymbol{T})$, the terms $\frac{\boldsymbol{B}}{\boldsymbol{B}^2} \times \nabla \boldsymbol{P}$, $\frac{\boldsymbol{B}}{\boldsymbol{B}^2} \times \boldsymbol{k_B}\boldsymbol{T}\nabla \boldsymbol{n}$, and $\frac{\boldsymbol{B}}{\boldsymbol{B}^2} \times \boldsymbol{k_B}\boldsymbol{n}\nabla \boldsymbol{T}$, labelled as $\boldsymbol{J}_{\nabla \boldsymbol{P}}$, $\boldsymbol{J}_{\nabla \boldsymbol{n}}$, and $\boldsymbol{J}_{\nabla \boldsymbol{T}}$, can be evaluated separately using the FIPS NTP data set. The parameters were averaged by bins of 0.1 $R_M$ ×0.1 $R_M$ ×0.1 $R_M$. **a, d, g.** The radial gradient of proton density (**a**), temperature (**d**), and the proton pressure (**g**). **b, e, h.** The azimuthal component of $\boldsymbol{J}_{\nabla \boldsymbol{n}}$ (**b**), $\boldsymbol{J}_{\nabla \boldsymbol{T}}$ (**e**), and $\boldsymbol{J}_{\nabla \boldsymbol{P}}$ (**h**). We label the azimuthal component of $\boldsymbol{J}_{\nabla \boldsymbol{n}}$, $\boldsymbol{J}_{\nabla \boldsymbol{T}}$, and $\boldsymbol{J}_{\nabla \boldsymbol{P}}$ as $\boldsymbol{J}_{\nabla \boldsymbol{n},\boldsymbol{\phi}}$, $\boldsymbol{J}_{\nabla \boldsymbol{T},\boldsymbol{\phi}}$, and $\boldsymbol{J}_{\nabla \boldsymbol{P},\boldsymbol{\phi}}$ respectively, and label the azimuthal component current density derived by $\boldsymbol{\nabla} \times \boldsymbol{B}$ as $J_{\phi}$. **c, f, i.** The ratios of $\boldsymbol{J}_{\nabla \boldsymbol{n},\boldsymbol{\phi}}/\boldsymbol{J}_{\boldsymbol{\phi}}$ (**c**), $\boldsymbol{J}_{\nabla \boldsymbol{T},\boldsymbol{\phi}}/\boldsymbol{J}_{\boldsymbol{\phi}}$ (**f**), and $\boldsymbol{J}_{\nabla \boldsymbol{P},\boldsymbol{\phi}}/\boldsymbol{J}_{\boldsymbol{\phi}}$ (**i**), if both currents are eastward in a bin.

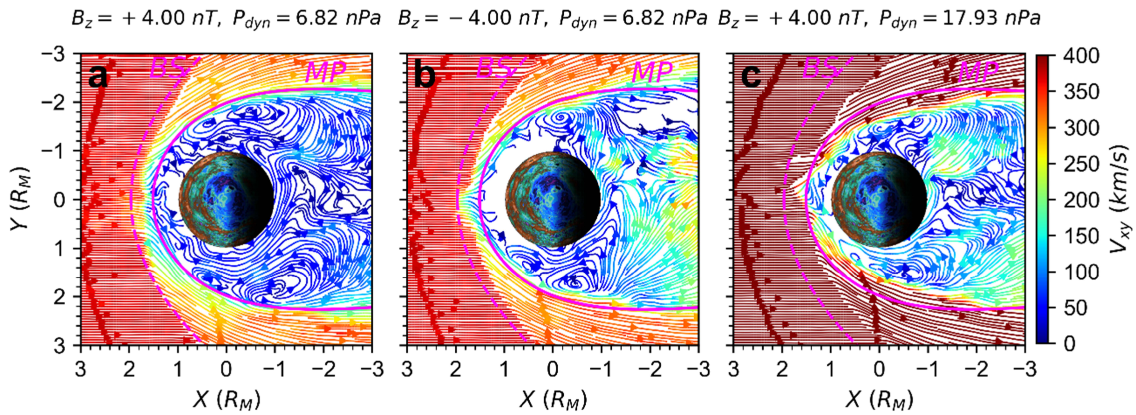


**Figure S7.** The simulated distributions of proton bulk velocity in the magnetic equatorial plane **($|z|$<0.05 $R_M$)**. **a, b, c.** The distribution of proton bulk velocity of three cases listed in Table 1, respectively. The streamlines of bulk velocity are colored by the velocity magnitude ($\boldsymbol{V_{xy}} = \sqrt{\boldsymbol{V_x^2} + \boldsymbol{V_y^2}}$). Dashed and solid magenta lines indicate the nominal shape of the bow shock and magnetopause, respectively.

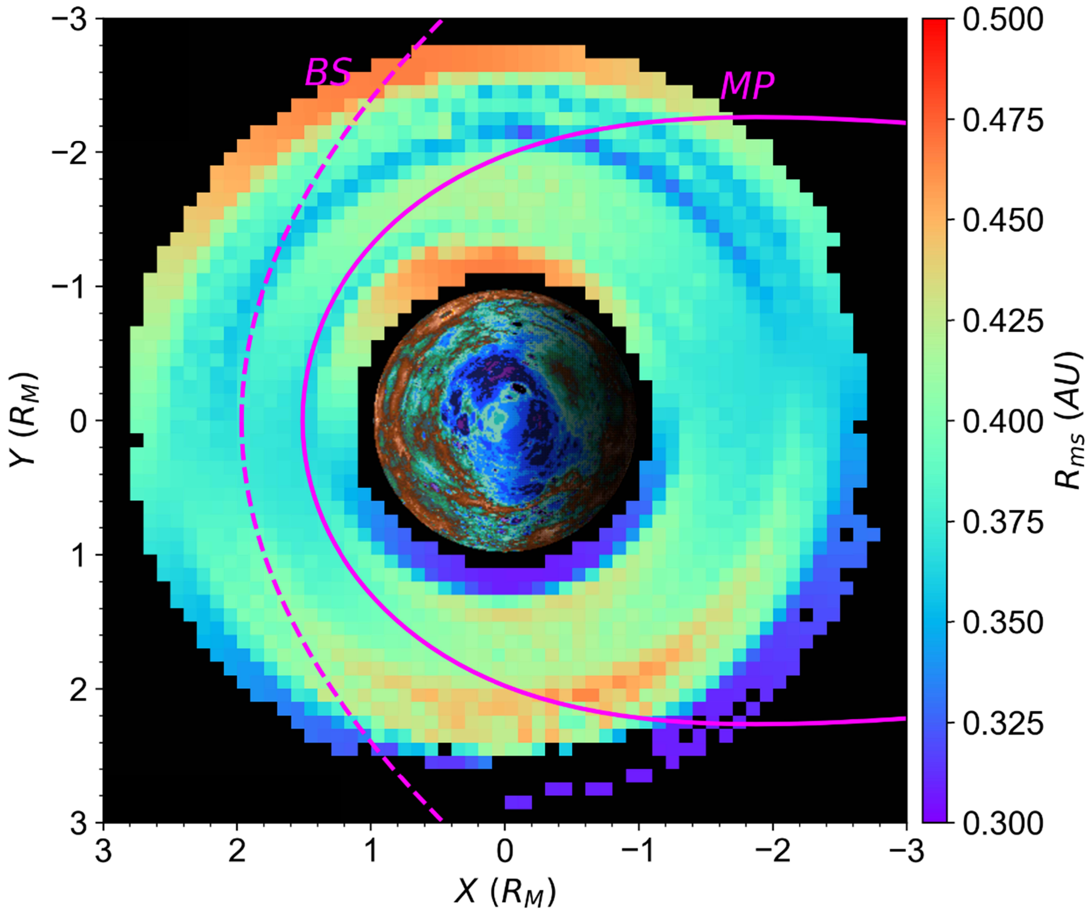


**Figure S8.** The distribution of MESSENGER's orbits in the cut of the magnetic equatorial plane ($|z|$<0.05 $R_M$). The bins are colored by the average heliocentric distance of spacecraft, $R_{ms}$.

**Table S1.** The input parameters of upstream solar wind for simulations. IMF $B_x$, IMF $B_y$ and IMF $B_z$ are the three components of the IMF along the x-axis, the y-axis, and the z-axis, respectively. IMF $B$ is the magnitude of IMF. $V_x$ is the flow speed of solar wind along the x-axis. $N_0$ is the number density of proton in the solar wind. $P_{dyn}$ is the dynamic pressure of the upstream solar wind. $\beta$ is the plasma Beta. $V_{CS}$ is the sound speed in the solar wind.

| | Case 1 | Case 2 | Case 3 | Case 4 | Case 5 |
|---|---|---|---|---|---|
| IMF $B_x$ (nT) | +17.55 | +17.55 | +17.55 | +17.85 | +17.85 |
| IMF $B_y$ (nT) | 0 | 0 | 0 | +2.31 | -2.31 |
| IMF $B_z$ (nT) | +4.00 | +4.00 | +4.00 | 0 | 0 |
| IMF $B$ (nT) | 18.00 | 18.00 | 18.00 | 18.00 | 18.00 |
| $V_x$ (km/s) | -370 | -600 | -370 | -370 | -370 |
| $N_0$ (#/cm$^3$) | 30.00 | 30.00 | 78.89 | 30.00 | 30.00 |
| $P_{dyn}$ (nPa) | 6.82 | 17.93 | 17.93 | 6.82 | 6.82 |
| $\beta$ | 0.90 | 0.90 | 2.37 | 0.90 | 0.90 |
| $V_{CS}$ (km/s) | 62.29 | 62.29 | 62.29 | 62.29 | 62.29 |